

# Earth's Future

## RESEARCH ARTICLE

10.1029/2021EF002173

# Future Changes in $\delta^{13}\text{C}$ of Dissolved Inorganic Carbon in the Ocean



### Key Points:

- An offline ocean model is used to predict the distribution of  $\delta^{13}\text{C}$  in DIC through 2100 under six scenarios
- In high emission scenarios, the Suess Effect strongly decreases  $\delta^{13}\text{C}$  in DIC, reversing vertical and horizontal  $\delta^{13}\text{C}$  gradients
- Estimates of the anthropogenic  $\text{CO}_2$  uptake by the ocean based on  $\delta^{13}\text{C}$  may become less reliable in the future



### Correspondence to:

H. Graven,  
[h.graven@imperial.ac.uk](mailto:h.graven@imperial.ac.uk)

### Citation:

Graven, H., Lamb, E., Blake, D., & Khatiwala, S. (2021). Future changes in  $\delta^{13}\text{C}$  of dissolved inorganic carbon in the ocean. *Earth's Future*, 9, e2021EF002173. <https://doi.org/10.1029/2021EF002173>

Received 4 MAY 2021  
Accepted 26 SEP 2021

Heather Graven<sup>1</sup> , Eleanor Lamb<sup>1</sup>, Daisy Blake<sup>1</sup>, and Samar Khatiwala<sup>2</sup> 

<sup>1</sup>Department of Physics, Imperial College London, London, UK, <sup>2</sup>Department of Earth Sciences, University of Oxford, Oxford, UK

**Abstract** Emissions of carbon dioxide from fossil fuel combustion are reducing the ratio  $^{13}\text{C}/^{12}\text{C}$ ,  $\delta^{13}\text{C}$ , in atmospheric  $\text{CO}_2$  and in the carbon in the ocean and terrestrial biosphere that exchanges with the atmosphere on timescales of decades to centuries. Future changes to fossil fuel emissions vary across different scenarios and may cause decreases of more than 6% in atmospheric  $\delta^{13}\text{C}$  between 1850 and 2100. The effects of these potential changes on the three-dimensional distribution of  $\delta^{13}\text{C}$  in the ocean have not yet been investigated. Here, we use an ocean biogeochemical-circulation model forced with a range of Shared Socioeconomic Pathway (SSP)-based scenarios to simulate  $\delta^{13}\text{C}$  in ocean dissolved inorganic carbon from 1850 to 2100. In the future, vertical and horizontal  $\delta^{13}\text{C}$  gradients characteristic of the biological pump are reduced or reversed, relative to the preindustrial period, with the reversal occurring in higher emission scenarios. For the highest emission scenario, SSP5-8.5, surface  $\delta^{13}\text{C}$  in the center of Pacific subtropical gyres falls from 2.2‰ in 1850 to  $-3.5$ ‰ by 2100. In lower emission scenarios,  $\delta^{13}\text{C}$  in the surface ocean decreases but then rebounds. The relationship between anthropogenic carbon ( $C_{\text{ant}}$ ) and  $\delta^{13}\text{C}$  in the ocean shows a larger scatter in all scenarios, suggesting that uncertainties in  $\delta^{13}\text{C}$ -based estimates of  $C_{\text{ant}}$  may increase in the future. These simulations were run with fixed physical forcing and ocean circulation, providing a baseline of predicted  $\delta^{13}\text{C}$ . Further work is needed to investigate the impact of climate-carbon cycle feedbacks on ocean  $\delta^{13}\text{C}$  changes.

**Plain Language Summary** The amount of  $\text{CO}_2$  absorbed in our oceans is an important factor in determining how much climate change will result from human activities. The more  $\text{CO}_2$  absorbed in the oceans, the less that is in the atmosphere warming the planet. However, more  $\text{CO}_2$  in the ocean causes more ocean acidification which can be harmful to marine organisms. When  $\text{CO}_2$  is absorbed by the ocean, the isotopic ratio  $^{13}\text{C}/^{12}\text{C}$  changes because fossil fuels contain less  $^{13}\text{C}$ . We conduct the first study of how future scenarios for fossil fuel emissions could affect the  $^{13}\text{C}/^{12}\text{C}$  ratio in the ocean by conducting computer simulations. These future changes can impact one of the methods that is used to quantify the  $\text{CO}_2$  absorbed by the ocean, which uses observations of the isotopic ratio of the dissolved carbon in the ocean. We find that there are large changes in the ratio of  $^{13}\text{C}/^{12}\text{C}$  in the ocean in future scenarios with high emissions, and that the method of estimating  $\text{CO}_2$  uptake by the ocean using  $^{13}\text{C}/^{12}\text{C}$  ratios may become less effective in the future.

## 1. Introduction

The isotopic ratio  $^{13}\text{C}/^{12}\text{C}$  in oceanic dissolved inorganic carbon (DIC) is influenced by physical, biological, and anthropogenic processes. The notation  $\delta^{13}\text{C}$  is typically used, representing deviations in the  $^{13}\text{C}/^{12}\text{C}$  ratio from that in a standard, Vienna Pee Dee Belemnite (VPDB). Marine biota preferentially take up  $^{12}\text{C}$  over  $^{13}\text{C}$  during photosynthesis (Goericke & Fry, 1994), thereby increasing  $\delta^{13}\text{C}$  of DIC in surface waters. The remineralization of particulate organic matter releases low  $\delta^{13}\text{C}$  carbon to DIC at depth, resulting in a gradient of high  $\delta^{13}\text{C}$  at the surface and a lower  $\delta^{13}\text{C}$  at depths. The observed  $\delta^{13}\text{C}$  patterns are largely dominated by this biological effect, but ocean circulation and air-sea gas exchange act to oppose and partially counteract the patterns driven by the biological pump (Eide, Olsen, Ninnemann, & Johannessen, 2017; Schmittner et al., 2013). The temperature dependence of fractionation during air-sea gas exchange (Broecker & Maier-Reimer, 1992; Zhang et al., 1995) and the degree of isotopic equilibration, which relates to the surface residence time of seawater, are also important in determining the ocean  $\delta^{13}\text{C}$  distribution (Khatiwala et al., 2019; Schmittner et al., 2013).

© 2021 The Authors. Earth's Future published by Wiley Periodicals LLC on behalf of American Geophysical Union. This is an open access article under the terms of the [Creative Commons Attribution License](https://creativecommons.org/licenses/by/4.0/), which permits use, distribution and reproduction in any medium, provided the original work is properly cited.

Since the Industrial Revolution, the combustion of fossil fuels has added low- $\delta^{13}\text{C}$  carbon originally derived from photosynthetically derived plant material to atmospheric  $\text{CO}_2$ .  $\delta^{13}\text{C}$  in atmospheric  $\text{CO}_2$  has decreased by nearly 2% since 1850 (Graven et al., 2017). This so-called “Suess Effect” influences  $\delta^{13}\text{C}$  in ocean DIC through air-sea gas exchange. Penetration of the anthropogenic low- $\delta^{13}\text{C}$  signal into the ocean has reduced  $\delta^{13}\text{C}$  of DIC in surface and recently ventilated waters, weakening the vertical gradient in  $\delta^{13}\text{C}$  over time (Eide, Olsen, Ninnemann, & Eldevik, 2017; Olsen & Ninnemann, 2010).

The observed change in  $\delta^{13}\text{C}$  of DIC has been exploited to estimate anthropogenic  $\text{CO}_2$  uptake by the ocean (Quay et al., 1992, 2003). This method constructs atmospheric and oceanic  $\text{CO}_2$  and  $\delta^{13}\text{CO}_2$  budgets to solve for the net oceanic and biospheric uptake rate of  $\text{CO}_2$ , where the observed depth-integrated change in ocean  $\delta^{13}\text{C}$  is a key element of the calculation. An oceanic  $\text{CO}_2$  uptake rate of  $1.5 \pm 0.6 \text{ GtC yr}^{-1}$  between 1970 and 1990 was estimated by Quay et al. (2003), taking into account different possible ways of applying the method. Recently, a new estimate of the oceanic  $\text{CO}_2$  uptake rate was produced by Eide, Olsen, Ninnemann, and Eldevik (2017), which emphasized uncertainties contributed not only by the uncertainty in the depth-integrated change in ocean  $\delta^{13}\text{C}$ , but also by uncertainties in the Suess Effect in the terrestrial biosphere and in marine organic carbon.

Other studies using  $\delta^{13}\text{C}$  observations in DIC have investigated biogeochemical cycling associated with marine ecosystems and air-sea gas exchange. Tagliabue and Bopp (2008) and Schmittner et al. (2013) used model simulations and model-data comparisons to quantify the impact of separate biological and physical processes on ocean  $\delta^{13}\text{C}$ . Krakauer et al. (2006) used observations of  $^{13}\text{C}$  together with  $^{14}\text{C}$  to investigate the global mean gas exchange velocity and its relationship with wind speed, suggesting that the wind speed dependence is close to linear rather than the commonly used quadratic dependence.

Future changes in  $\delta^{13}\text{C}$  of atmospheric  $\text{CO}_2$  depend on fossil fuel emissions and the natural carbon cycle's response to higher  $\text{CO}_2$  and climate change (Graven et al., 2020; Köhler, 2016). The potential large-scale deployment of  $\text{CO}_2$  removal by Bioenergy with Carbon Capture and Storage (BECCS) in some future scenarios also has a significant impact because BECCS will act to preferentially remove  $^{12}\text{C}$  from the atmosphere-ocean-biosphere system through photosynthesis and burial of biofuel-derived  $\text{CO}_2$  (Graven et al., 2020; Köhler, 2016). Future scenarios based on the Shared Socioeconomic Pathways (SSPs) being used in the sixth Coupled Model Intercomparison Project (CMIP6) indicate a range of  $-8\%$  to  $-10\%$  by 2050 and a range of  $-7\%$  to  $-13\%$  by 2100 for six different scenarios (Graven et al., 2020). These predictions of atmospheric  $\delta^{13}\text{C}$  were made using a simple carbon cycle model with a one-dimensional ocean model.

Potential future changes to the three-dimensional distribution of  $\delta^{13}\text{C}$  in the ocean have not yet been explored, even though atmospheric changes of  $+1.5\%$  to  $-4.5\%$  between now and 2100 would have a large impact on  $\delta^{13}\text{C}$  of DIC. In this study, we present future simulations of  $\delta^{13}\text{C}$  in DIC for the six SSP-based scenarios presented in Graven et al. (2020). We use an ocean biogeochemical model run with physical forcing (temperature, salinity, and winds) and ocean circulation fixed at their preindustrial values to isolate the effects of changing atmospheric  $\text{CO}_2$  and  $\delta^{13}\text{C}$ . The model is evaluated against observation-based estimates of preindustrial and modern  $\delta^{13}\text{C}$ . We present the simulated surface ocean  $\delta^{13}\text{C}$  distribution and vertical gradients in  $\delta^{13}\text{C}$  in 2100. We also present the projected changes in  $\delta^{13}\text{C}$  between 2020 and 2050 to describe the expected changes that will be observed by ship-based measurements in the coming decades. Finally, we show the relationships between the change in  $\delta^{13}\text{C}$  of DIC (the oceanic Suess Effect) and the anthropogenic  $\text{CO}_2$  concentration to quantify how the use of  $\delta^{13}\text{C}$ -DIC observations to trace anthropogenic  $\text{CO}_2$  may be affected by atmospheric  $\delta^{13}\text{C}$  changes.

## 2. Methods

We simulated  $^{13}\text{C}$  with the Model of Ocean Biogeochemistry and Isotopes (MOBI), an NPZD (Nutrient, Phytoplankton, Zooplankton, Detritus) marine ecosystem and carbon cycle model. MOBI features three limiting nutrients (dissolved nitrogen, phosphorus, and iron), two phytoplankton functional groups, and one zooplankton class (Schmittner & Somes, 2016). Other tracers include DIC, dissolved and particulate organic matter, oxygen, and alkalinity. The iron cycle is driven by fluxes from atmospheric dust, sediments, and hydrothermal vents (Muglia et al., 2017). MOBI is coupled to the Transport Matrix Method (TMM), a numerical framework for efficient offline tracer simulations (Khatiwala, 2007, 2018; Khatiwala et al., 2005).

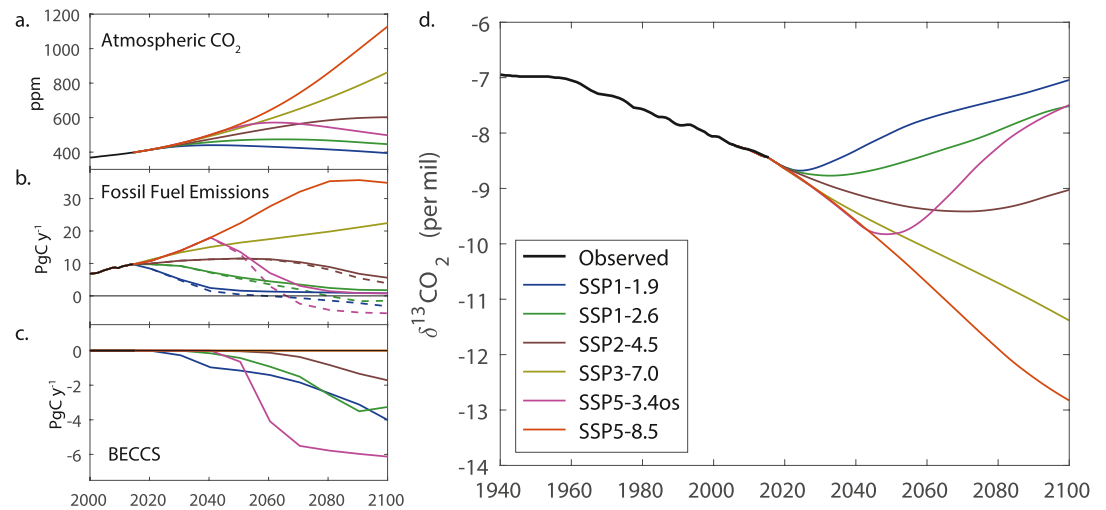


**Figure 1.** Future scenarios of atmospheric CO<sub>2</sub> (a), fossil fuel emissions (b), Bioenergy with Carbon Capture and Storage (BECCS) (c), and δ<sup>13</sup>C in atmospheric CO<sub>2</sub>. Reproduced from Graven et al. (2020).

In this study, MOBI-TMM is driven by monthly mean transport matrices and other fields, including temperature, salinity, sea ice, and winds, from a preindustrial configuration (Khatiwala et al., 2019; Muglia & Schmittner, 2015) of the University of Victoria Earth System Climate Model (UVic ESCM; version 2.9) (Weaver et al., 2001). UVic ESCM is a three-dimensional ocean general circulation model, with a resolution of 1.8° × 3.6° × 19 layers, coupled to an atmospheric energy-moisture balance and dynamic-thermodynamic sea ice model. The transport matrices and other fields have been derived from averages for each calendar month from a preindustrial simulation of the UVic ESCM, and thus our simulations are for a fixed preindustrial ocean circulation.

Carbon isotopes are tracked through all model components in MOBI and their treatment is described in detail in Schmittner et al. (2013). Briefly, fractionation during air-sea gas exchange is modeled via a constant kinetic fractionation factor and a temperature-dependent equilibrium fractionation factor for the gaseous CO<sub>2</sub> to DIC transformation (Zhang et al., 1995). The aqueous CO<sub>2</sub> to particulate organic carbon transformation during photosynthesis involves an equilibrium fractionation factor that is a function of the partial pressure of CO<sub>2</sub> in surface water (Popp et al., 1989). Values for the various fractionation factors and parameters involved in CO<sub>2</sub> gas-exchange are identical to those in Schmittner et al. (2013). The only difference is that we used a slightly higher coefficient in the quadratic parameterization of the gas transfer velocity with wind speed (0.272 cm/h s<sup>2</sup>/m<sup>2</sup> instead of 0.2528 cm/h s<sup>2</sup>/m<sup>2</sup>). This results in a global mean CO<sub>2</sub> transfer velocity of 17 cm/hr (Khatiwala et al., 2018) rather than ~15.8 cm/h.

We specify preindustrial (1850) ocean δ<sup>13</sup>C by the final values of a 5000-year spinup run with atmospheric CO<sub>2</sub> and δ<sup>13</sup>C fixed at 1850 values. Simulations for the historical period (1850–2015) were run with observed atmospheric CO<sub>2</sub> and δ<sup>13</sup>C records from Meinshausen et al. (2017) and Graven et al. (2017). Future simulations were run for 2015 to 2100 for six scenarios based on the SSPs (O'Neill et al., 2017). For the future simulations, atmospheric CO<sub>2</sub> was downloaded from input4mips (<https://esgf-node.llnl.gov/projects/input4mips/>) and δ<sup>13</sup>C was taken from Graven et al. (2020) (also available at input4mips). Figure 1 shows the atmospheric CO<sub>2</sub> and δ<sup>13</sup>C forcings used in the simulations over 1940–2100. For all simulations, the circulation and physical forcing fields (temperature, salinity, sea ice, and winds) were kept fixed at their preindustrial values. Thus, only changes caused by CO<sub>2</sub> uptake were included: changes in CO<sub>2</sub> solubility from changes in the buffer factor and changes in fractionation from changes in the fraction of DIC as carbonate ions. No changes in ocean circulation, productivity, or temperature-dependent solubility or fractionation were simulated.

### 3. Results

#### 3.1. Model Evaluation

We compare  $\delta^{13}\text{C}$  simulated by MOBI-TMM with reconstructions of  $\delta^{13}\text{C}$  in DIC based on observations from ocean cruise surveys, specifically, a  $\delta^{13}\text{C}$  climatology for the modern ocean (1994) and an estimate for the preindustrial period (1850), taken from Eide, Olsen, Ninnemann, Eldevik, and Johannessen (2017). Direct comparisons are made by interpolating the climatology ( $1^\circ \times 1^\circ$ ) onto the model grid. We calculate the simulated Suess Effect in 1994, 2050, and 2100 by subtracting  $\delta^{13}\text{C}$  in 1850 from those years.

Figures 2a–2d show the simulated  $\delta^{13}\text{C}$  in DIC for the preindustrial (1850) and modern (1994) periods, along the sections A16 (Atlantic Ocean,  $30^\circ\text{W}$ ) and P16 (Pacific Ocean,  $150^\circ\text{W}$ ). In 1850,  $\delta^{13}\text{C}$  is highest in the subtropical gyres, particularly in the Atlantic, and decreases from  $>2\%$  in the gyres to less than  $1\%$  in the Southern Ocean (Figures 2a and 2b). North Atlantic Deep Water has relatively high  $\delta^{13}\text{C}$  of  $1\%$ – $1.5\%$  while Pacific Deep Water has the lowest  $\delta^{13}\text{C}$  of about  $-0.5\%$ . The distribution is mainly driven by the biological pump, where marine productivity enriches surface waters by preferentially assimilating  $^{12}\text{C}$  while deeper waters are reduced by the remineralization of low- $\delta^{13}\text{C}$  sinking organic matter (Goericke & Fry, 1994). Physical influences from ocean circulation and gas exchange are also important to the  $\delta^{13}\text{C}$  distribution and generally oppose the influence of the biological pump (Eide, Olsen, Ninnemann, & Johannessen, 2017; Schmittner et al., 2013).

In 1994, the  $\delta^{13}\text{C}$  pattern is similar but  $\delta^{13}\text{C}$  at shallow depths has decreased and the vertical gradients have weakened due to the Suess Effect (Figures 2c and 2d; Olsen & Ninnemann, 2010). The magnitude of the Suess Effect in 1994 is simulated to be between  $0\%$  and  $-0.8\%$ , with the strongest changes in the subtropical gyres where vertical transport is weak and water remains in contact with the atmosphere longer (Figures 2e and 2f).

Compared with the preindustrial climatology of Eide, Olsen, Ninnemann, and Johannessen (2017), the vertical gradients in MOBI-TMM are stronger (Figures 2g and 2h).  $\delta^{13}\text{C}$  in the subtropical gyres and North Atlantic Deep Water is about  $0.5\%$  higher, and  $\delta^{13}\text{C}$  in Antarctic Intermediate Water and Bottom Water is about  $0.3\%$  lower than Eide, Olsen, Ninnemann, and Johannessen (2017).  $\delta^{13}\text{C}$  in Pacific Deep Water shows a small positive bias. Positive biases compared with 1990–2005 data in mid-depths were also found in Schmittner et al. (2013) and appeared to be associated with biases in DIC concentration. Overall, the model appears to have a stronger effect of the biological pump on  $\delta^{13}\text{C}$  (or weaker effect of the opposing processes) than in the estimate from Eide, Olsen, Ninnemann, and Johannessen (2017). Eide et al. report a  $\pm 20\%$  uncertainty in their estimate, which is generally comparable to the differences with MOBI-TMM.

Comparing the change in  $\delta^{13}\text{C}$  from 1850 to 1994 between MOBI-TMM and Eide, Olsen, Ninnemann, and Eldevik (2017)'s estimate shows the bias in the Suess Effect (Figures 2i and 2j). The Suess Effect is weaker in North Atlantic Deep Water and North Pacific Intermediate Water in MOBI-TMM, but stronger between 300 and 1000 m depth between  $40^\circ\text{S}$  and  $20^\circ\text{N}$ . Eide, Olsen, Ninnemann, and Eldevik (2017) report a  $\pm 15\%$  uncertainty in their estimate of the Suess Effect. The differences in Figures 2i and 2j are larger than  $\pm 15\%$  in several places, however, this fractional uncertainty estimate is quite small ( $\leq 0.15\%$ ) and it is fixed to the pattern of the Suess Effect in Eide, Olsen, Ninnemann, and Eldevik (2017). It is expected that MOBI-TMM's Suess Effect should be somewhat stronger away from the surface compared with Eide et al.'s reconstruction, as the latter base their estimate on CFC-12 data, so that the effect of fossil fuel emissions before the 1940s will be underrepresented. The general pattern of stronger  $\delta^{13}\text{C}$  change in MOBI-TMM may indicate that the Suess Effect is being ventilated too rapidly. In this case, the Suess Effect would be expected to be underestimated near the surface, which is evident in (Figures 2i and 2j), although Eide et al.'s estimate have significant uncertainty for depths  $< 200$  m. Based on this comparison, our future simulations, which include only transient changes due to atmospheric  $\text{CO}_2$  and  $\delta^{13}\text{C}$  trends (i.e., Suess Effect changes), may underestimate the  $\delta^{13}\text{C}$  changes near the surface and overestimate the changes deeper in the ocean by ventilating the atmospheric signals too rapidly.

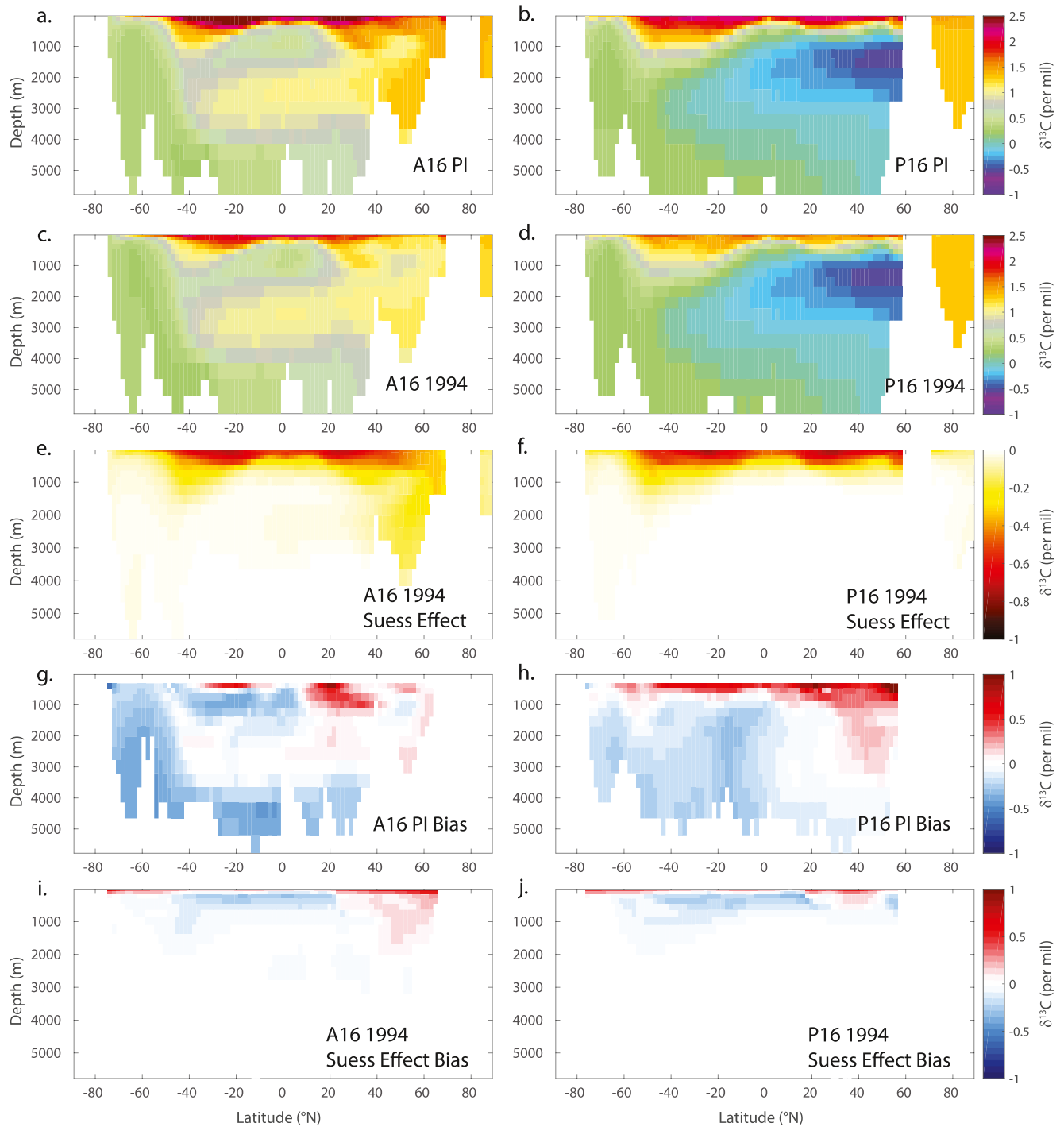


**Figure 2.** The  $\delta^{13}\text{C}$  simulated for hydrographic sections through the Atlantic and Pacific Oceans, A16 and P16, for preindustrial conditions from the year 1850 (a, b) and for the year 1994 (c, d). The difference between the year 1994 and the preindustrial distributions, termed the Suess Effect, is shown in (e, f). Biases in the preindustrial  $\delta^{13}\text{C}$  distribution (g, h) and in the Suess Effect (i, j) in comparison to Eide, Olsen, Ninnemann, and Johannessen (2017) and Eide, Olsen, Ninnemann, and Eldevik (2017) were made by interpolating Eide et al.'s data onto the same grid as MOBI-TMM. Comparisons start below 200 m in (g, h).

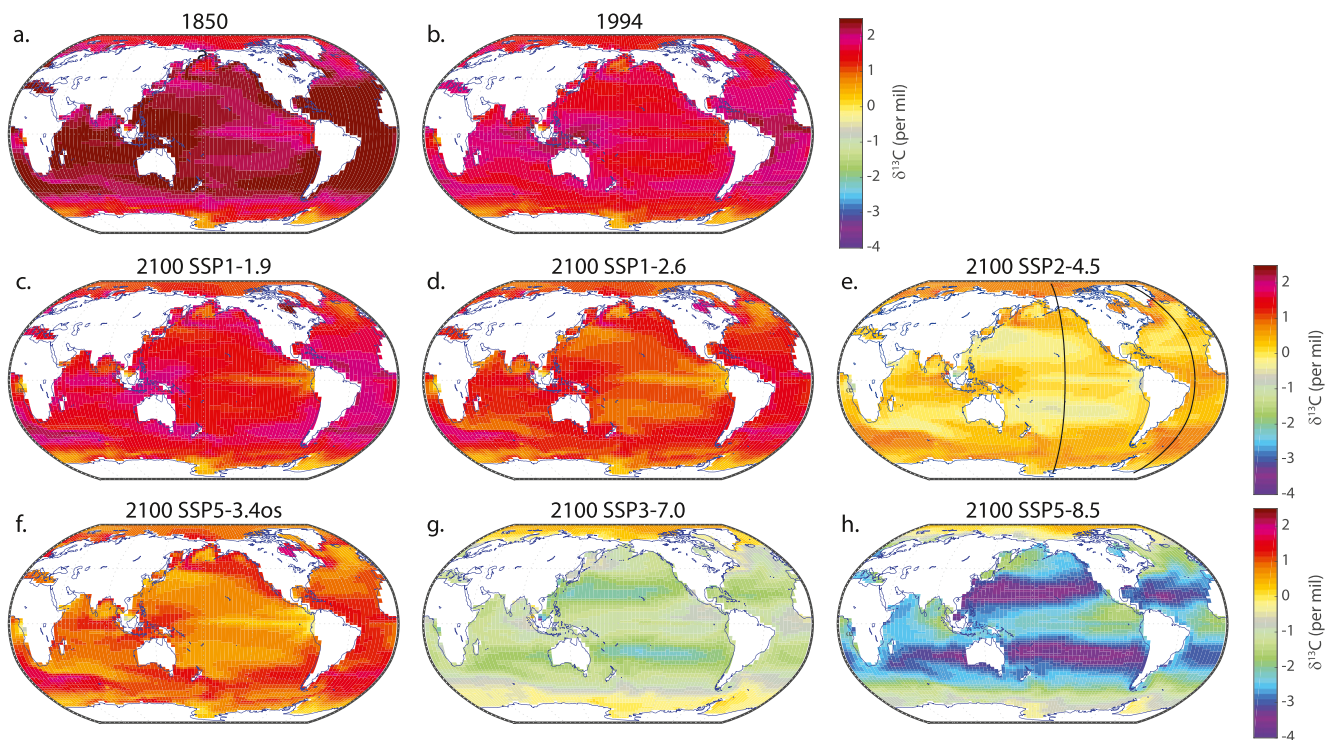


**Figure 3.** Simulated  $\delta^{13}\text{C}$  (%) in the surface ocean for 1850 (a) and 1994 (b) and for the six SSPs (c–h). Black lines in panel (e) show  $150^\circ$  and  $30^\circ\text{W}$  corresponding to the P16 and A16 sections presented in Figures 2, 4, and 5.

### 3.2. Simulated Ocean Surface $\delta^{13}\text{C}$ Distributions in 2100

The simulated distributions of  $\delta^{13}\text{C}$  at the ocean surface in 1850, 1994, and 2100 for the six scenarios are shown in Figure 3. Between 1850 and 1994,  $\delta^{13}\text{C}$  decreased by up to 1% in the subtropical gyres. Smaller decreases are simulated in the tropics and high latitudes where there is more vertical mixing, upwelling, and/or isotopic equilibration is limited by short surface residence times or sea ice.

In the lowest emission scenario, SSP1-1.9, the surface  $\delta^{13}\text{C}$  distribution in 2100 is largely similar to 1994 (Figure 3c). Tropical and higher latitude  $\delta^{13}\text{C}$  has decreased, as compared with 1994. Even though in this scenario the atmospheric  $\delta^{13}\text{C}$  reached a minimum in the 2020s and rebounded to  $-7\%$  in 2100, near to the 1950 level (Figure 1), the surface  $\delta^{13}\text{C}$  distribution is still slightly lower than in 1994.

The scenarios SSP1-2.6 and SSP3-4.0s have atmospheric  $\delta^{13}\text{C}$  in 2100 of about  $-7.5\%$  (Figure 1), and their surface  $\delta^{13}\text{C}$  distributions are generally 0.5% or more below SSP1-1.9 (Figures 3d and 3f). SSP3-4.0s is lower than SSP1-2.6 because atmospheric  $\delta^{13}\text{C}$  reached a deeper minimum of nearly  $-10\%$ , with significantly more fossil fuels burned and more BECCS deployed (Figure 1). In SSP3-4.0s, large areas of the surface ocean are between 0% and 0.5%, which was the lowest value simulated in the surface ocean in 1850.

In SSP2-4.5, most of the surface ocean is around 0% (Figure 3e), so that the horizontal gradients and the range of surface values are much smaller than in 1850. Here, the minimum values are now actually in the subtropical gyres in the Pacific Ocean.

The patterns in  $\delta^{13}\text{C}$  have completely reversed in SSP3-7.0 and SSP5-8.5, compared with the preindustrial and modern distributions. Gradients of roughly 2% in magnitude are observed between the subtropical gyres and high latitudes ( $>50^\circ$ ) in SSP3-7.0, but the sign is the opposite to 1850 and 1994. In the highest emission scenario, SSP5-8.5, these gradients are as large as 3.5%. The subtropical gyres and midlatitudes are also significantly lower than the tropics.

In SSP5-8.5, nearly all of the surface ocean in 2100 has  $\delta^{13}\text{C}$  lower than  $-0.6\%$ , which was the minimum in ocean  $\delta^{13}\text{C}$  observed in Pacific Deep Water in 1994 (Eide, Olsen, Ninnemann, & Johannessen, 2017).

Moreover, in the surface subtropical gyres, values less than  $-3\%$  are simulated under this scenario. In SSP3-7.0, all regions apart from the high latitudes have  $\delta^{13}\text{C}$  lower than  $-0.6\%$  in 2100, with minimum values lower than  $-2\%$  simulated in the subtropical gyres.

### 3.3. Simulated Vertical $\delta^{13}\text{C}$ Distributions in 2100

The future changes in  $\delta^{13}\text{C}$  in the surface ocean presented in the previous section imply very large changes in the vertical gradients in  $\delta^{13}\text{C}$  in the high emissions scenarios but moderate changes in lower emission scenarios. Figure 4 shows the Atlantic and Pacific vertical sections A16 and P16 in 2100 for the six scenarios, which can be compared with the simulated preindustrial and 1994 A16 and P16 sections in Figures 2a–2d (note the different ranges in color bars).

SSP1-1.9 and SSP1-2.6 exhibit similar vertical distributions in 2100 (Figures 4a–4d), which are similar to, but weaker than, the gradients in 1850 and 1994.  $\delta^{13}\text{C}$  decreases by  $0\%$ – $2\%$  between the surface and about 1000 m depth, and by  $0.2\%$ – $1\%$  between the surface and North Atlantic Deep Water or Antarctic Bottom Water. SSP5-3.4os (Figures 4g and 4h) also shows  $\delta^{13}\text{C}$  decreasing with depth, but with even weaker gradients than for SSP1-1.9 and SSP1-2.6. Despite the atmospheric  $\delta^{13}\text{C}$  dropping to nearly  $-10\%$  by mid-century, the rapid rebound of atmospheric  $\delta^{13}\text{C}$  substantially increases  $\delta^{13}\text{C}$  again in shallow waters by 2100. In these three scenarios, the distributions show the combined effect of the decreases in atmospheric  $\delta^{13}\text{C}$  until the minima in 2020–2050, which have reduced the  $\delta^{13}\text{C}$  at intermediate depths, and the subsequent rises in atmospheric  $\delta^{13}\text{C}$ , which increase  $\delta^{13}\text{C}$  in decadal ventilated waters.

SSP2-4.5 in 2100 shows very little difference between  $\delta^{13}\text{C}$  at the surface and below 1000 m depth, apart from the North Pacific, with minimum  $\delta^{13}\text{C}$  at 500–1000 m depth outside of the Southern Ocean and North Pacific (Figures 4e and 4f). In this scenario, the preindustrial  $\delta^{13}\text{C}$  gradients have largely been canceled by the Suess Effect.

The SSP3-7.0 and SSP5-8.5 scenarios show dramatic decreases in  $\delta^{13}\text{C}$  in shallow waters and in North Atlantic Deep Water in 2100 that reverse the preindustrial  $\delta^{13}\text{C}$  gradients in the ocean (Figures 4i–4l). In SSP3-7.0, the low values of  $-1\%$  to  $-2\%$  at the surface (Figure 3) extend to 1000 m depth outside of the Southern Ocean. In SSP5-8.5 low values of  $-1\%$  to  $-2\%$  extend below 1000 m and into the Southern Ocean.  $\delta^{13}\text{C}$  below  $-3\%$  is found in the subtropical gyres to a few hundred meters depth. In SSP3-7.0, the vertical gradients are up to  $2.5\%$ , which is similar in magnitude to the preindustrial gradients, but opposite in sign. In SSP5-8.5 they are up to  $4\%$ , not only opposite in sign, but much stronger than the preindustrial gradients (about  $2.5\%$  or less), showing the very large magnitude of the Suess Effect in this scenario.

Changes in the Arctic Ocean, particularly the western Arctic, are relatively small in all scenarios, reflecting the longer timescales of ventilation there, particularly as no change in sea ice cover is included in the simulations. Minimum Arctic  $\delta^{13}\text{C}$  is about  $1\%$  in SSP5-8.5 in 2100 for A16 and P16.

### 3.4. Simulated $\delta^{13}\text{C}$ Changes in the Next 30 Years

To get an idea of the range of potential changes in  $\delta^{13}\text{C}$  that will be observed by research cruise surveys in the next three decades, we plot the simulated  $\delta^{13}\text{C}$  changes between 2020 and 2050 for the A16 and P16 vertical sections in the lowest emission scenario, SSP1-1.9, and the highest, SSP5-8.5, in Figure 5. In SSP5-8.5, decreases of up to  $1\%$  are simulated near the surface, apart from the high latitudes. Decreases of less than  $0.5\%$  are simulated in North Atlantic Deep Water and in mode and intermediate waters. No change is simulated outside of these relatively well-ventilated regions, as expected from the 30 years timescale and fixed circulation, physical forcing, and productivity used in the simulations. For SSP1-1.9, the changes at the surface are close to zero everywhere, with decreases of less than  $0.5\%$  simulated in North Atlantic Deep Water and in the thermocline above 1000 m depth. Particularly for the lowest emission scenario, the detection of small changes across repeated measurements over 5–10 years may challenge our current observation capabilities.

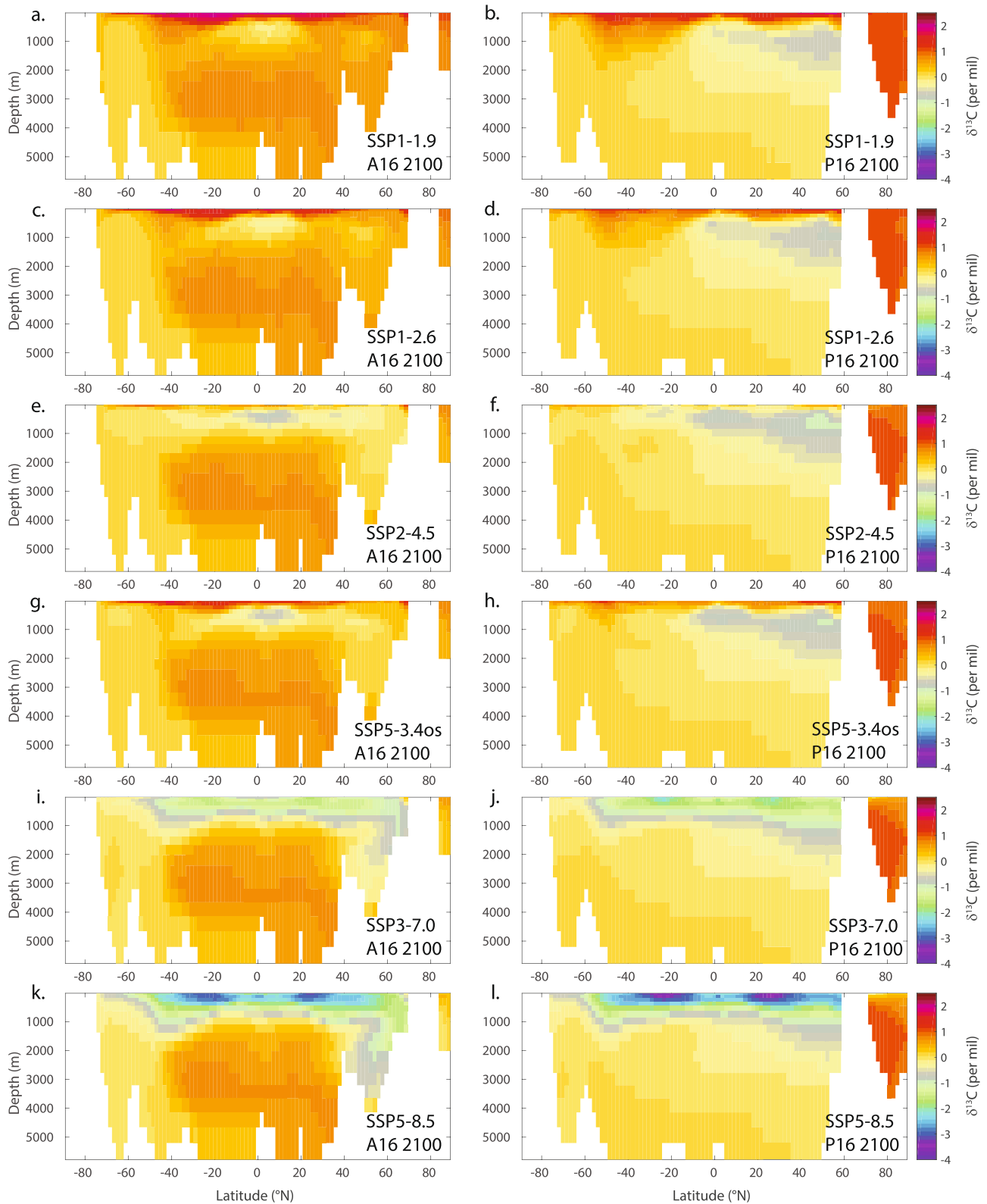


**Figure 4.** Simulated  $\delta^{13}\text{C}$  (%) in 2100 for the A16 and P16 vertical sections in the six SSPs.



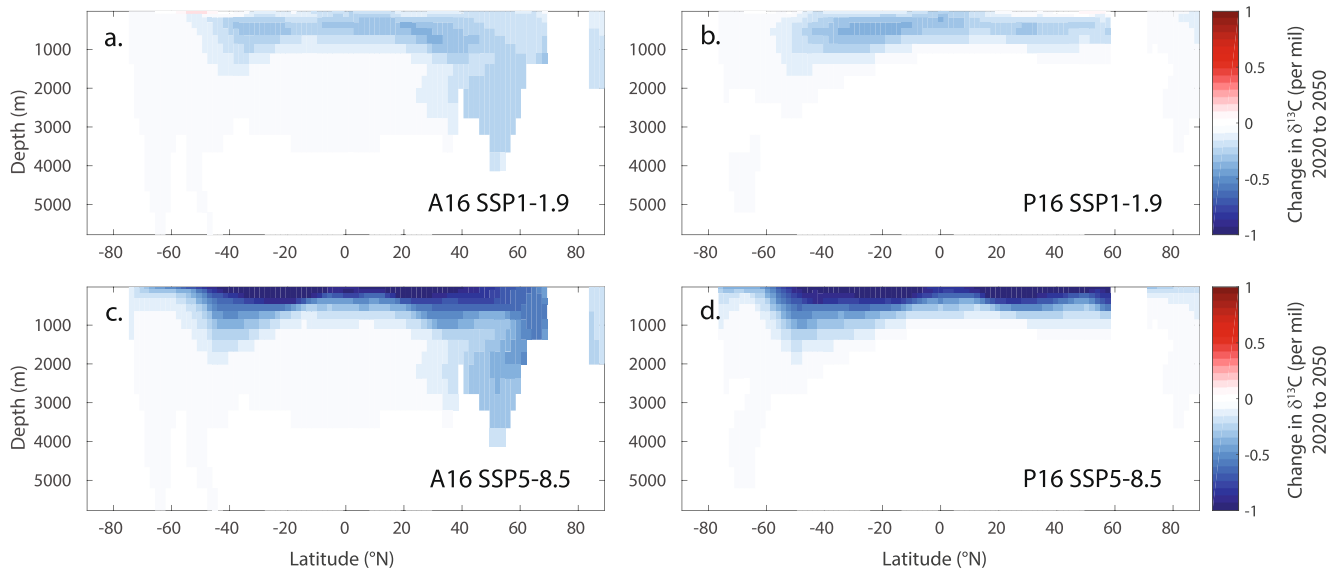


**Figure 5.** Simulated  $\delta^{13}\text{C}$  (%) changes between 2020 and 2050 for the A16 and P16 vertical sections in SSP1-1.9 and SSP5-8.5.

### 3.5. Future Relationship Between $\delta^{13}\text{C}$ Change and Anthropogenic $\text{CO}_2$

Finally, we investigate how the relationship between the  $^{13}\text{C}$  Suess Effect (the change in  $\delta^{13}\text{C}$  (%) since 1850) and the anthropogenic carbon concentration ( $C_{\text{ant}}$ , the change in DIC since 1850) evolve from 1994 (Figure 6a) to 2050 and 2100 in SSP1-1.9 and SSP5-8.5 (Figures 6b, 6c, 6e, and 6f). Figure 6d shows the relationship between  $\delta^{13}\text{C}$  in atmospheric  $\text{CO}_2$  and atmospheric  $\text{CO}_2$  concentration between 1850 and 2100. In atmospheric  $\text{CO}_2$ ,  $\delta^{13}\text{C}$  declined by approximately 2‰ between 1850 and 2015 while atmospheric  $\text{CO}_2$  concentration increased by approximately 120 ppm (Figure 6d). A similar slope is found in the high emission

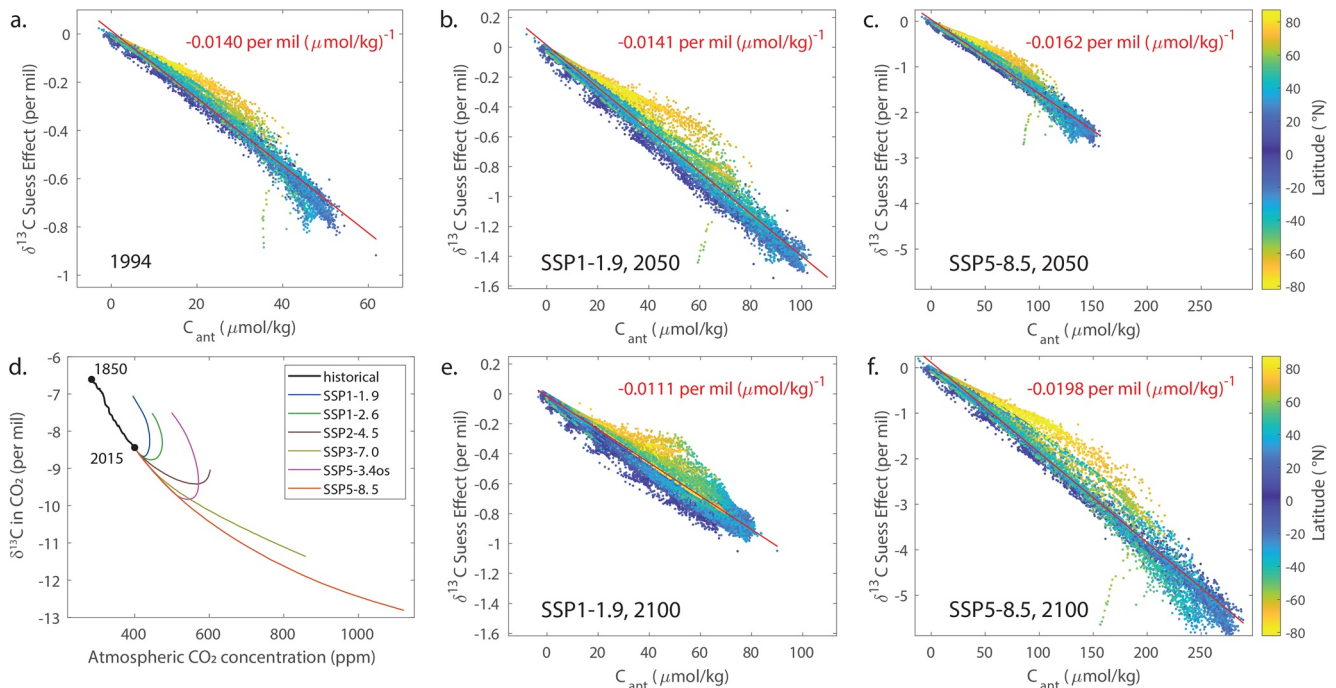


**Figure 6.** Simulated change in  $\delta^{13}\text{C}$  since 1850 versus simulated change in DIC for 1994 (a) and for 2050 and 2100 in SSP1-1.9 (b, e) and SSP5-8.5 (c, f). Colors indicate latitude and a regression fit is shown in red. The scatterplots show 20% of the model grid cells. Panel (d) shows the relationship between  $\delta^{13}\text{C}$  in atmospheric  $\text{CO}_2$  and the atmospheric  $\text{CO}_2$  concentration over 1850–2015 and for each of the SSPs from 2015 until 2100.

scenarios SSP5-8.5 and SSP3-7.0 up to about 500 ppm, after which point the slope gradually weakens. In the four other scenarios, the trends reverse as fossil fuel emissions decrease toward and drop below zero in some scenarios. In these scenarios, there is a period where  $\delta^{13}\text{C}$  is changing more quickly than atmospheric  $\text{CO}_2$  concentration, relative to the 1850–2015 period.  $\delta^{13}\text{C}$  begins increasing while atmospheric  $\text{CO}_2$  continues to rise, then atmospheric  $\text{CO}_2$  concentration “catches up” and  $\delta^{13}\text{C}$  and  $\text{CO}_2$  concentration again change with a similar slope as for the increase between 1850 and 2015 but with a reversal in the trends. The future trends in  $\delta^{13}\text{C}$  in atmospheric  $\text{CO}_2$  and atmospheric  $\text{CO}_2$  concentration reflect changes in fossil fuel emissions and carbon uptake and assimilation of the  $\delta^{13}\text{C}$  perturbation by the natural carbon cycle, as well as the preferential removal of  $^{12}\text{C}$  by BECCS in low-emission scenarios.

In 1994, the overall simulated relationship between the  $^{13}\text{C}$  Suess Effect and  $C_{\text{ant}}$  is  $-0.0140\%$  per  $\mu\text{mol}/\text{kg}$  (Figure 6a), indistinguishable from the data-based estimates in Eide, Olsen, Ninnemann, and Eldevik (2017). The slope is weaker in the high latitudes where the shorter residence time of water at the ocean surface limits isotopic equilibration with the atmosphere (McNeil et al., 2001).

In SSP1-1.9, the  $^{13}\text{C}$  Suess Effect to  $C_{\text{ant}}$  slope is similar to 1994 in 2050 but it is weaker in 2100, at  $-0.0111\%$  per  $\mu\text{mol}/\text{kg}$  (Figures 6b and 6e). The maximum values of  $C_{\text{ant}}$  have decreased and minimum values of the  $^{13}\text{C}$  Suess Effect have increased between 2050 and 2100 as atmospheric  $\text{CO}_2$  concentration decreased and atmospheric  $\delta^{13}\text{C}$  increased (Figures 1 and 6d). Importantly, the scatter in the relationship between the  $^{13}\text{C}$  Suess Effect and  $C_{\text{ant}}$  is roughly 100% larger in absolute magnitude in 2050 and 2100, with a greater difference between the tropical and high latitude slopes. This indicates that future observations of the  $^{13}\text{C}$  Suess Effect will exhibit larger spatial heterogeneity, likely increasing uncertainties related to the extrapolation of discrete data and potentially requiring more observations to apply methods for estimating ocean  $C_{\text{ant}}$  via the  $^{13}\text{C}$  Suess Effect.

In SSP5-8.5, the  $^{13}\text{C}$  Suess Effect to  $C_{\text{ant}}$  slope is stronger than in 1994 in 2050 ( $-0.0162\%$  per  $\mu\text{mol}/\text{kg}$ ) and even stronger in 2100 ( $-0.0198\%$  per  $\mu\text{mol}/\text{kg}$ ). As in SSP1-1.9, the scatter in the relationship between the  $^{13}\text{C}$  Suess Effect and  $C_{\text{ant}}$  is roughly 100% larger in absolute magnitude in 2050 and 2100.

#### 4. Discussion and Conclusions

The future spatio-temporal evolution of  $\delta^{13}\text{C}$  of ocean DIC up to 2100 has been modeled for the first time. The potential future changes in atmospheric  $\delta^{13}\text{C}$  over this century are likely to change the three-dimensional distribution of  $\delta^{13}\text{C}$  of ocean DIC from its preindustrial and present state. In high emission scenarios the Suess Effect overwhelms the effect of the biological pump and reverses the vertical and horizontal gradients in  $\delta^{13}\text{C}$  from their preindustrial state by 2100 (Figures 3 and 4). For medium emission scenarios, the Suess Effect nearly cancels the preindustrial gradients to produce a much more uniform  $\delta^{13}\text{C}$  distribution. Near-term changes to 2050 may be as small as a few tenths of a per mil, even at shallow depths of a few hundred meters, requiring high precision and compatibility in ocean  $\delta^{13}\text{C}$  measurements made in different time periods and by different laboratories.

Studies exploiting the observed  $^{13}\text{C}$  Suess Effect in the ocean to estimate anthropogenic  $\text{CO}_2$  uptake (Eide, Olsen, Ninnemann, & Eldevik, 2017; Heimann & Maier-Reimer, 1996; Quay et al., 1992, 2003) are likely to be affected by future changes. We found that in both the lowest and highest emission scenarios, the scatter in the relationship between the Suess Effect and  $C_{\text{ant}}$  becomes  $\sim 100\%$  larger than in 1994, likely increasing the uncertainty in the method or requiring more comprehensive global coverage in oceanic  $\delta^{13}\text{C}$  observations.

Projected future changes in the Suess Effect can be expected to impact studies of marine ecosystems using oceanic  $\delta^{13}\text{C}$  observations (Schmittner et al., 2013; Tagliabue & Bopp, 2008). As the Suess Effect gets stronger in some future scenarios, it will have more of a counteracting influence on the effects of the biological pump. Studies using oceanic  $\delta^{13}\text{C}$  observations to study marine ecosystems will need to account for larger influences of the Suess Effect and, potentially, larger uncertainties in these influences. It appears that in all future scenarios, the regional differences in the relationship between the Suess Effect and  $C_{\text{ant}}$  will increase (Figure 6), which may make it more difficult to reliably account for the Suess Effect in these studies.

The comparison between our simulated Suess Effect in 1994 and the observation-based estimate from Eide, Olsen, Ninnemann, and Eldevik (2017) suggests that our future simulations may ventilate the atmospheric

signals too rapidly, underestimating the  $\delta^{13}\text{C}$  changes near the surface and overestimating them deeper in the ocean. Thus, future changes in the surface  $\delta^{13}\text{C}$  distribution and vertical  $\delta^{13}\text{C}$  gradients may be even more dramatic than those simulated here, since more of the low- $\delta^{13}\text{C}$  signal would be concentrated at the surface.

Our simulations only consider the impact of changing atmospheric composition without including the potential effects of future changes in marine productivity, isotopic fractionation, ocean circulation, or sea ice cover. For example, a common feature in historical and high-emission scenarios of Earth System Models, including UVic ECSM, is a slowing of the meridional overturning circulation, which can reduce the transport of anthropogenic  $\text{CO}_2$  and isotopic perturbations into the deep ocean, with implications for their vertical distributions (Khatiwala et al., 2018). These effects may have a substantial influence on future air-sea fluxes of  $^{13}\text{C}$ , relative to  $^{12}\text{C}$ , and the evolving ocean distribution of  $\delta^{13}\text{C}$ , and they should be investigated in future work.

### Data Availability Statement

Computing resources were provided by the University of Oxford Advanced Research Computing (ARC) facility (<http://dx.doi.org/10.5281/zenodo.22558>) and the ARCHER UK National Supercomputing Service (<http://www.archer.ac.uk/>). Simulation output is available at <https://doi.org/10.5281/zenodo.5519285>. Model codes are available from Khatiwala (2018) <https://doi.org/10.5281/zenodo.1246300>.

### Acknowledgments

HG acknowledges support from the Leverhulme Trust. SK was supported by UK NERC grants NE/M020835/1 and NE/P019218/1.

### References

- Broecker, W. S., & Maier-Reimer, E. (1992). The influence of air and sea exchange on the carbon isotope distribution in the sea. *Global Biogeochemical Cycles*, 6(3), 315–320. <https://doi.org/10.1029/92gb01672>
- Eide, M., Olsen, A., Ninnemann, U. S., & Eldevik, T. (2017). A global estimate of the full oceanic  $^{13}\text{C}$  Suess effect since the preindustrial. *Global Biogeochemical Cycles*, 31(3), 492–514. <https://doi.org/10.1002/2016gb005472>
- Eide, M., Olsen, A., Ninnemann, U. S., Eldevik, T., & Johannessen, T. (2017). Climatological distributions of  $\delta^{13}\text{C}$  of dissolved inorganic carbon in the global oceans. <https://doi.org/10.1594/PANGAEA.872004>
- Eide, M., Olsen, A., Ninnemann, U. S., & Johannessen, T. (2017). A global ocean climatology of preindustrial and modern ocean. *Global Biogeochemical Cycles*, 31(3), 515–534. <https://doi.org/10.1002/2016gb005473>
- Goericke, R., & Fry, B. (1994). Variations of marine plankton  $\delta^{13}\text{C}$  with latitude, temperature, and dissolved  $\text{CO}_2$  in the world ocean. *Global Biogeochemical Cycles*, 8(1), 85–90.
- Graven, H., Allison, C. E., Etheridge, D. M., Hammer, S., Keeling, R. F., Levin, I., et al. (2017). Compiled records of carbon isotopes in atmospheric for historical simulations in CMIP6. *Geoscientific Model Development*, 10(12), 4405–4417. <https://doi.org/10.5194/gmd-10-4405-2017>
- Graven, H., Keeling, R. F., & Rogelj, J. (2020). Changes to carbon isotopes in atmospheric  $\text{CO}_2$  over the industrial era and into the future. *Global Biogeochemical Cycles*, 34(11), e2019GB006170.
- Heimann, M., & Maier-Reimer, E. (1996). On the relations between the oceanic uptake of and its carbon isotopes. *Global Biogeochemical Cycles*, 10(1), 89–110. <https://doi.org/10.1029/95gb03191>
- Khatiwala, S. (2007). A computational framework for simulation of biogeochemical tracers in the ocean. *Global Biogeochemical Cycles*, 21, GB3001. <https://doi.org/10.1029/2007GB002923>
- Khatiwala, S. (2018). Transport matrix method software for ocean biogeochemical simulations. <https://doi.org/10.5281/zenodo.1246300>
- Khatiwala, S., Graven, H., Payne, S., & Heimbach, P. (2018). Changes to the air-sea flux and distribution of radiocarbon in the ocean over the 21st century. *Geophysical Research Letters*, 45(11), 5617–5626. <https://doi.org/10.1029/2018gl078172>
- Khatiwala, S., Schmittner, A., & Muglia, J. (2019). Air-sea disequilibrium enhances ocean carbon storage during glacial periods. *Science Advances*, 5(6), eaaw4981. <https://doi.org/10.1126/sciadv.aaw4981>
- Khatiwala, S., Visbeck, M., & Cane, M. (2005). Accelerated simulation of passive tracers in ocean circulation models. *Ocean Modelling*, 9, 51–69. <https://doi.org/10.1016/j.ocemod.2004.04.002>
- Köhler, P. (2016). Using the Suess effect on the stable carbon isotope to distinguish the future from the past in radiocarbon. *Environmental Research Letters*, 11(12), 124016. <https://doi.org/10.1088/1748-9326/11/12/124016>
- Krakauer, N. Y., Randerson, J. T., Primeau, F. W., Gruber, N., & Menemenlis, D. (2006). Carbon isotope evidence for the latitudinal distribution and wind speed dependence of the air-sea gas transfer velocity. *Tellus B: Chemical and Physical Meteorology*, 58(5), 390–417. <https://doi.org/10.1111/j.1600-0889.2006.00223.x>
- McNeil, B. I., Matear, R. J., & Tilbrook, B. (2001). Does carbon 13 track anthropogenic in the southern ocean? *Global Biogeochemical Cycles*, 15(3), 597–613. <https://doi.org/10.1029/2000gb001352>
- Meinshausen, M., Vogel, E., Nauels, A., Lorbacher, K., Meinshausen, N., Etheridge, D. M., et al. (2017). Historical greenhouse gas concentrations for climate modelling (CMIP6). *Geoscientific Model Development*, 10(5), 2057–2116. <https://doi.org/10.5194/gmd-10-2057-2017>
- Muglia, J., & Schmittner, A. (2015). Glacial Atlantic overturning increased by wind stress in climate models. *Geophysical Research Letters*, 42, 9862–9868. <https://doi.org/10.1002/2015GL064583>
- Muglia, J., Somes, C., Nickelsen, L., & Schmittner, A. (2017). Combined effects of atmospheric and seafloor iron fluxes to the glacial ocean. *Paleoceanography*, 32, 1204–1218. <https://doi.org/10.1002/2016PA003077>
- Olsen, A., & Ninnemann, U. (2010). Large gradients in the Preindustrial North Atlantic Revealed. *Science*, 330(6004), 658–659. <https://doi.org/10.1126/science.1193769>

- O'Neill, B. C., Kriegler, E., Ebi, K. L., Kemp-Benedict, E., Riahi, K., Rothman, D. S., et al. (2017). The roads ahead: Narratives for shared socioeconomic pathways describing world futures in the 21st century. *Global Environmental Change*, 42, 169–180. <https://doi.org/10.1016/j.gloenvcha.2015.01.004>
- Popp, B. N., Takigiku, R., Hayes, J. M., Louda, J. W., & Baker, E. W. (1989). The post-Palaeozoic chronology and mechanism of  $^{13}\text{C}$  depletion in primary marine organic matter. *American Journal of Science*, 289, 436–454. <https://doi.org/10.2475/ajs.289.4.436>
- Quay, P. D., Sonnerup, R., Westby, T., Stutsman, J., & McNichol, A. (2003). Changes in the  $^{13}\text{C}/^{12}\text{C}$  of dissolved inorganic carbon in the ocean as a tracer of anthropogenic  $\text{CO}_2$  uptake. *Global Biogeochemical Cycles*, 17(1), 4–1. <https://doi.org/10.1029/2001gb001817>
- Quay, P. D., Tilbrook, B., & Wong, C. S. (1992). Oceanic uptake of fossil fuel : Carbon-13 evidence. *Science*, 256(5053), 74–79. <https://doi.org/10.1126/science.256.5053.74>
- Schmittner, A., Gruber, N., Mix, A. C., Key, R. M., Tagliabue, A., & Westberry, T. K. (2013). Biology and air-sea gas exchange controls on the distribution of carbon isotope ratios ( $\delta^{13}\text{C}$ ) in the ocean. *Biogeosciences*, 10(9), 5793–5816. <https://doi.org/10.5194/bg-10-5793-2013>
- Schmittner, A., & Somes, C. J. (2016). Complementary constraints from carbon ( $^{13}\text{C}$ ) and nitrogen ( $^{15}\text{N}$ ) isotopes on the glacial ocean's soft-tissue biological pump. *Paleoceanography*, 31, 669–693. <https://doi.org/10.1002/2015PA002905>
- Tagliabue, A., & Bopp, L. (2008). Towards understanding global variability in ocean carbon-13. *Global Biogeochemical Cycles*, 22(1). <https://doi.org/10.1029/2007gb003037>
- Weaver, A., Eby, M., Wiebe, E., Bitz, C., Duffy, P., Ewen, T., et al. (2001). The UVic Earth System Climate Model: Model description, climatology, and applications to past, present and future climates. *Atmosphere-Ocean*, 39(4), 361–428. <https://doi.org/10.1080/07055900.2001.9649686>
- Zhang, J., Quay, P. D., & Wilbur, D. O. (1995). Carbon isotope fractionation during gas-water exchange and dissolution of  $\text{CO}_2$ . *Geochimica et Cosmochimica Acta*, 59(1), 107–114. [https://doi.org/10.1016/0016-7037\(95\)91550-d](https://doi.org/10.1016/0016-7037(95)91550-d)